Electricity generation and bivalent copper reduction as a function of operation time and cathode electrode material in microbial fuel cells

Dan Wu[a]

Liping Huang[a, *]

lipinghuang@dlut.edu.cn

Xie Quan[a]

Gianluca Li Puma[b, **]

g.lipuma@lboro.ac.uk

[a]Key Laboratory of Industrial Ecology and Environmental Engineering, Ministry of Education (MOE), School of Environmental Science and Technology, Dalian University of Technology, Dalian 116024, China

[b]Environmental Nanocatalysis & Photoreaction Engineering, Department of Chemical Engineering, Loughborough University, Loughborough LE11 3TU, United Kingdom

*Corresponding author.

**Corresponding author.

Abstract

The performance of carbon rod (CR), titanium sheet (TS), stainless steel woven mesh (SSM) and copper sheet (CS) cathode materials are investigated in microbial fuel cells (MFCs) for simultaneous electricity generation and Cu(II) reduction, in multiple batch cycle operations. After 12 cycles, the MFC with CR exhibits 55% reduction in the maximum power density and 76% increase in Cu(II) removal. In contrast, the TS and SSM cathodes at cycle 12 show maximum power densities of 1.7 (TS) and 3.4 (SSM) times, and Cu(II) removal of 1.2 (TS) and 1.3 (SSM) times higher than those observed during the first cycle. Diffusional resistance in the TS and SSM cathodes is found to appreciably decrease over time due to the copper deposition. In contrast to CR, TS and SSM, the cathode made with CS is heavily corroded in the first cycle, exhibiting significant reduction in both the maximum power density and Cu(II) removal at cycle 2, after which the performance stabilizes. These results demonstrate that the initial deposition of copper on the cathodes of MFCs is crucial for efficient and continuous Cu(II) reduction and electricity generation over prolonged time. This effect is closely associated with the nature of the cathode material. Among the materials examined, the SSM is the most effective and inexpensive cathode for practical use in MFCs.

Keywords: Microbial fuel cell; Cu(II) reduction; Electricity generation; Cathode electrode; Deposited copper

1 Introduction

Bioelectrochemical systems (BESs) including microbial fuel cells (MFCs) and microbial electrolysis cells (MECs) are regarded as new, sustainable and effective technologies for the recovery of metals from wastes and wastewaters [1]. Among the variety of heavy metals that can be recovered by BESs from wastes and wastewaters, the recovery of Cu(II) has attracted significant attention due to its wide presence in acid mine drainage wastewaters [2,3]. The reduction of Cu(II) can be achieved on the abiotic cathodes of two-chamber MFCs, since this metal has a relatively high redox potential (+0.286 V vs. standard hydrogen electrode, SHE) relative to the redox potential of the organic matter (ca. –0.30 V for acetate under standard conditions vs. SHE) in the anolyte [4]. MFCs with various operating volumes and experimental conditions, as well as different architectures, have been explored for more efficient Cu(II) reduction and higher electricity generation with varying degrees of success, as shown in Table 1 [3–13]. However, these studies do not investigate the performance of the cell in multiple batch cycles, and the long-term stability of MFCs for Cu(II) reduction, even though the longevity of the MFCs is crucial for its commercial application.

Table 1 Summary of the studies applying BESs for Cu(II) recovery, including the process parameters and the relevant recovery efficiencies obtained.

Electron donor	Reactor	Anode	Cathode	Operation mode	Anodic working volume (L)	Cathodic working volume	Initial pH in	Initial Cu(II) concentration	Operation time (h)	Reduction rate (mg L^{-1} h^{-1})^a	Product	Maximum power (W m^{-3})^b	Power produced (kWh kg^{-1} Cu)	References

Substrate	MFC type	Anode	Cathode	Operation	(L)	(L)	catholyte	(mg L⁻¹)			Metal			Ref.
Acetate	Two-chamber MFC	Carbon fiber brush	Graphite rod	Batch	0.014	0.028	2.0	800	24	29	Cu	33.6	1.16	[3]
Acetate	Two-chamber MFC	Graphite plate	Graphite foil	Batch	0.8	0.8	3.0	1000	168	5.94	Cu	2.2	0.37	[4]
Acetate	Two-chamber MFC	Graphite felt	Graphite disk	Batch	6	10	2.0	60	480	0.115	Cu	0.059	0.51	[5]
Glucose	Membrane-free baffled MFC	Graphite plate	Graphite plate	Batch	1.0	1.0	7.0	200–6400	144	1.3–5.2	Cu + Cu$_2$O	0.05–0.31	0.04–0.06	[6]
Glucose	Membrane-free MFC	Graphite felt	Graphite disk	Batch	1.0	1.0	4.7	196–6412	264	1.4–3.3	Cu + Cu$_2$O	0.26–0.34	0.08–0.25	[7]
Acetate	Two-chamber MFC	Graphite felt	Graphite plate	Batch	0.125	0.0625	3.0–9.0	350	8–12	28.0–36.8	Cu + Cu$_2$O	20.5	0.56–0.73	[8]
Acetate	Four-chamber MFC	Carbon felt	Graphite plate	Batch	0.049	0.049	3.0	100–800	22	4.54–34.2	Cu + Cu$_2$O	2.8–7.9	0.23–0.62	[9]
Acetate	Two-chamber MFC	Carbon felt	Copper plate	Batch	Not provided	10	3.0	2000	24	75	Cu	5.5	0.081	[10]
Acetate	Two-chamber MFC	Graphite felt	Carbon rod	Batch	0.025	0.025	2.0	50	4	3.18	Cu	4.0	0.31	[11]
Acetate	Two-chamber MEC	Carbon felt	Titanium wire	Batch	Not provided	0.080	2 M HCl	800	2–4, 20–24	Cu: 8.9; Pb: 2.3; Cd: 2.8; Zn: 1.2	Cu, Pb, Cd, Zn	0–1.7[c]	None	[12]
Acetate	Two-chamber MEC	Graphite brush	Carbon cloth coated with Pt	Batch	0.028	0.035	2.9	320	32–96	Cu: 8; Ni: 3.7; Fe: 6.3	Cu, Ni, H$_2$	1.0[c]	None	[13]

[a] Calculated on the basis of cathode working volume (mg L^{-1} h^{-1}).

[b] Calculated on the basis of cathode working volume (W m^{-3}).

[c] Applied voltage (V).

Non-corrosive, carbon-based materials such as carbon cloth, carbon rod, graphite felt, graphite foil, graphite rod, graphite plate, as well as, metals of titanium wire and copper plate have been used as cathodes in MFCs for Cu(II) reduction [3–13]. In view of a practical environmental application, during the prolonged operation of MFCs results in increasing amount of copper are is unavoidably deposited on the surface of the cathodes, and as a result, the interaction of the cathode material with the deposited copper becomes crucial for determining the long-term performance of the cell. Copper is an excellent conductor that interacts with various materials. It promotes enhanced electrocatalytic activity towards oxygen and hydrogen peroxide reduction reactions in conventional electrochemical processes, due to the enlarged surface roughness and to the presence of new active sites [14–16]. Films of CuO on stainless steel mesh also exhibit efficient catalytic activities for propene oxidation [17] while copper phthalocyanine performs as platinum catalysis for oxygen reduction reaction in MFCs [18]. With regards to the capacitance of the electrodes, nanocrystals of copper can function with mesoporous activated carbons similarly as noble metals such as Pt and Pd, giving rise to substantial enhancement of the capacitance of carbonaceous electrodes [15]. Based on the intrinsic excellent charactersistics of copper, Motos et al. [10] successfully decreased the internal resistance of MFCs through, utilizing by coupling a copper plate cathode together with an anion exchange membrane, and a carbon felt anode. and Using a short distance between the electrodes, and thus achieve a the copper reduction rate of was 75 mg L^{-1} h^{-1} and a the maximum power production of was 5.5 W m^{-3} at a high initial Cu(II) concentration of 2000 mg L^{-1} [10] (Table 1). RThe metal reduction rates of Cu(II) reduction and power production would be reasonably expected to increase in proportion to the concentration of Cu(II) in the water. Together with considering the However, the performance of the electrode materials commonly used in MFCs, including carbon rod (CR), titanium sheet (TS) and stainless steel woven mesh (SSM), the is significantly influenced by the deposited copper. with these excellent characters may affect which with its excellent physico-chemical characteristics may alter the electrochemical behaviour of the the surface of the cathode and thus alter the and, as a result, the overall subsequent performance of MFCs. which to our knowledge This effect has not been systematically investigated in literature.

In this study, species specimens of CR, TS and SSM are investigated as cathode materials in MFCs for simultaneous electricity generation and Cu(II) reduction, in multiple batch cycle operations. For comparison convenience, Furthermore,

copper sheet (CS) is additionally used as one ~~further~~ cathode material ~~for~~to assess the MFC system performance. The effect of ~~the~~ deposited copper on system performance is elucidated by linear sweep voltammetry (LSV), scanning electronic microscopy (SEM), energy dispersive X-ray spectrometry (EDS), X-ray diffraction (XRD) and electrochemical impedance spectroscopy (EIS). The maximum power density and Cu(II) reduction in the MFCs were compared with those obtained with different batch cycle operations under otherwise identical conditions. The circuital current, the anodic columbic efficiency (CE) and the cathodic CE were employed to assess system performance.

2 Materials and methods

2.1 Reactor setup

Two-chamber MFCs (duplicates) were used in all experiments, with the chambers separated by a cation exchange membrane (CMI-7000 Membranes International, Glen Rock, NJ). The anodes were made with porous graphite felt (1.5 × 1.5 × 1.0 cm, Sanye Co., Beijing, China). The working volumes of the anode and cathode compartments were 20 mL each. The cathodes were made with CR (Chijiu Duratight Carbon Co., China), TS, SSM and CS (Qingyuan Co., China) and were all exposing the same surface area of 8 cm^2. The compositions of cathode electrodes ~~were~~is listed in Table S1. The cathode materials were first mechanically polished with abrasive papers and then cleaned with ethanol and deionized water before their installation in the MFCs [19,20].

2.2 Inoculation and operation

The anodes were inoculated from the anodes of previous operating MFCs running on acetate for faster anodic biofilm acclimation [3,11,19,20]. The composite of anolyte was as previously described [21]. The anolyte was sparged with ultrapure N_2 gas for 15 min, prior to transfer into ~~the~~ reactors. For anode acclimation, deionized water was used as catholyte and CR as cathode electrodes, with an external resistor of 510 Ω. After six-cycle anolyte refreshments with each lasting 2–3 days, the catholyte was replaced by aqueous $CuCl_2$ at a Cu(II) concentration of 50 mg L^{-1}. Prior to adding the Cu(II)-catholyte into the cathode chambers, the catholyte was thoroughly sparged with ultrapure N_2 gas for 15 min in order to exclude the effect of dissolved oxygen on Cu(II) reduction [4]. ~~A~~The acclimation period was completed after another 2–3 refreshments with stable and repeatable voltage output~~, the acclimation period was completed~~. New electrodes of CR, TS, SSM and CS were then alternatively installed in the cathode chambers for multiple batch cycle operations with each cycle (defined as each refreshment in catholyte) lasting 6 h. Unless otherwise stated, the same cathodes were always used for multiple batch cycle operations. All reactors were operated in fed-batch mode and all experiments were run in duplicate and at room temperature (20 ± 3 °C). The inoculation and solution replacements were performed in an anaerobic glove box (YQX-II, Xinmiao, Shanghai).

2.3 Measurements and analyses

Total chemical oxygen demand (COD) was measured using standard methods. Cu(II) species were analyzed by an atomic absorption spectrophotometer (AAnalyst 700, PerkinElmer). A SEM (QUANTA450, FEI company, USA) equipped with an EDS (X-MAX 20 mm^2–50 mm^2, Oxford Instruments, UK), and XRD (XRD-6000, Shimadzu LabX, Japan) measurements were used to examine the morphologies of the electrodes after Cu(II) reduction, as well as the crystal products. The sample preparation was strictly performed at N_2 atmosphere [22]. The cathode and anode potentials were monitored by a data logger using an automatic data acquisition system (PISO-813, Hongge Co., Taiwan). Power density was normalized to the cathode chamber working volume (W m^{-3}). LSV was conducted using a potentiostat (CHI 760C, Chenhua, Shanghai), with two electrode system of a working electrode (cathode electrode) and a counter electrode (anode electrode). The LSV was performed from open circuital potential (OCP) to 0.0 V at a scan rate of 0.1 mV s^{-1}. Cathodic LSV and EIS were performed using the same potentiostat with three electrode system consisted of a working electrode (cathode electrode) in the cathode, an Ag/AgCl reference electrode (195 mV vs. SHE) setting 1 cm away from the cathode in the cathodic chamber and a Pt foil (2 × 4 cm) counter electrode in the anodic chamber. The cathodic LSV was performed from cathodic open electrode potential (0.45 V for CR, 0.22 V for TS and 0.32 V for SSM) to –0.08 V (vs. SHE) at a scan rate of 0.1 mV s^{-1}. Since working potentials of all cathode electrodes were more positive than –0.08 V (vs. SHE), the lowest scanned potential of –0.08 V (vs. SHE) can guarantee the range of all cathodic potentials under the experimental conditions.

The catholyte was always composed of 50 mg L^{-1} Cu(II) at an initial pH of 2.0 and a solution conductivity of 5.0 mS cm^{-1}. This low initial pH of 2.0 was more approachable to practical acid mine wastewaters [2,3]. All the potentials reported in this study were in volts (V) units relative to a SHE. One-way ANOVA in SPSS 19.0 was used to analyze the differences among the data, and all of the data indicated significance levels of $p < 0.05$.

~~Due to the much more~~The large amount of data recorded during each polarisation experiment, is reported with discretisation by deleting 18 data in each interval between two symbols, to facilitate the visual reading of the results.~~recorded during each polarisation experiment, is reported with discretisation by deleting 18 data in each interval between two symbols, to facilitate the visual reading of the results.and for the sake of a clear comparison of the LSV results, in most cases, each two data with ignoring their interval 18 data were collected and reported~~. Impedance analysis were conducted at polarized conditions close to ~~the~~ MFC cathode operating potentials, which were –0.1 V and 0 V (vs. SHE, for different cathodes) over a frequency range of 100 kHz ~~to~~ 10 mHz with a sinusoidal perturbation of 10 mV amplitude [19]. The equivalent circuit and detailed value of different resistances were obtained through Zsimpwin software and normalized to the projected area of the cathodes [23].

2.4 Calculation

Cu(II) reduction was expressed as ~~the~~ net change of concentration divided by the initial concentration (%). The ~~columbic efficiency CE~~(CE) in the anodic chamber (CE_{an}, %) was calculated according to Eq. (1) and the CE in the cathodic chamber (CE_{ca}, %) was defined as the ratio of electrons used for Cu(II) reduction and the electrons extracted from the organic oxidation in the anodic chamber (Eq. (2)).

$$CE_{an} = \frac{\int Idt}{F \times \frac{4 \times \Delta COD \times V_{an}}{32}} \times 100\%$$

(1)

$$CE_{ca} = \frac{(\Delta C \times V_{ca}/65) \times 2 \times F}{1000 \times \int Idt} \times 100\%$$

(2)

where I is the circuital current (A); t is a set operational time (s); ΔCOD is the corresponding cumulative COD values in the anolytes over the operational period of t hours (g L^{-1}); V_{an} and V_{ca} are the anode and cathode working volumes, respectively (L); ΔC is the change of Cu(II) concentrations during the operational time t (mg L^{-1}); 2 and 4 are the molar numbers of electrons required for Cu(II) reduction and oxygen reduction, respectively (mol mol^{-1}); 65 is the molecular weight of copper (g mol^{-1}); 32 is the molecular weight of O_2 (g mol^{-1}) and F is the Faraday constant (96485 C mol^{-1} e^{-}).

3 Results and discussion

3.1 Polarization curves as a function of time

Maximum power density with the CR cathode gradually increased from 1.9 W m^{-3} (7.1 A m^{-3}) at cycle 2 to 2.6 W m^{-3} (9.4 A m^{-3}) at cycle 12 (Fig. 1A). An exceptional high power of 3.7–4.6 W m^{-3} (7.6–24.3 A m^{-3}) was observed at cycle 1, mainly ascribed to the occurrence of a power overshoot probably due to ions and substrate limitations [24]. Similarly, TS (Fig. 1D) and SSM (Fig. 1G) cathodes exhibited a gradual increase in the maximum power densities, reaching 3.1 W m^{-3} (11.6 A m^{-3}) and 6.5 W m^{-3} (26.9 A m^{-3}) in cycle 12, 1.7 and 3.4 times as high as those in cycle 1. These results illustrate the dependency of the maximum power density on both cathode material and operational time. At cycle 14, no further increase in the maximum power density was observed for all CR, TS and SSM cathodes (Fig. 1A, D, G and J). While an insoluble copper crust had sufficiently covered the cathodes at cycle 12, the reduction of some deposited copper from the SSM cathodes at cycle 14 explained the increase in ohmic resistance (Fig. 1G and H). In contrast to these results, CS cathode showed a significantly higher maximum power of 10.8 W m^{-3} (33.8 A m^{-3}) at cycle 1 (Fig. 1J) which decreased to and stabilized at 3.2 W m^{-3} (10.6 A m^{-3}) over successive cycles, implying the occurrence of heavy CS corrosion at cycle 1. This result was consistent with the very a recent report study of Cu(II) reduction on the copper plate cathodes in MFCs [10].
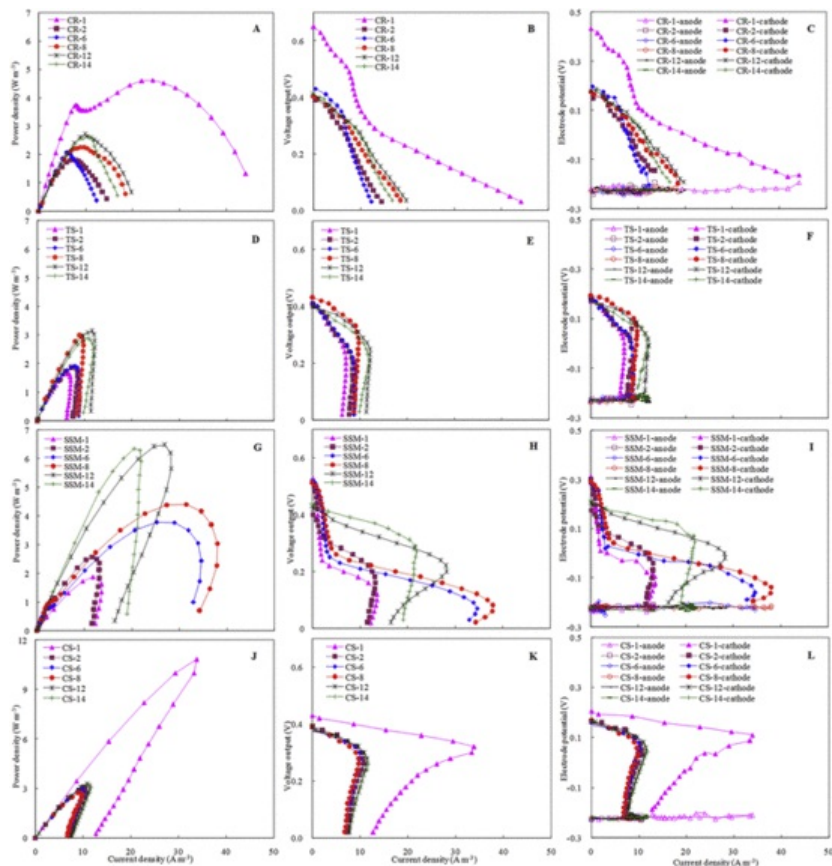
Fig. 1 Power density (A, D, G and J), voltage output (B, E, H and K), and anodic and cathodic potentials (C, F, I and L) ~~from~~in MFCs with ~~cathodes of~~ CR (A, B and C), TS (D, E and F), SSM (G, H and I), and CS (J, K and L) cathodes as a function of time (each cycle lasted 6 h).

Concomitant with power density, the OCPs with CR cathodes sharply decreased from 0.65 V at cycle 1 to 0.40 V at cycle 2, stabilizing at 0.40–0.43 V thereafter (Fig. 1B), whereas cathodes with TS (Fig. 1E) and CS (Fig. 1K) always exhibited OCPs in the range 0.40–0.43 V over time. Although SSM cathodes produced higher OCPs of 0.50–0.52 V during the initial 8 cycles, the overpotentials during this period was apparently high (Fig. 1H), resulting in a comparatively lower power production (Fig. 1G).

~~P~~The cathodic ~~p~~otentials of all ~~material cathodes~~cathode materials ~~changed~~varied much more than the anod~~e~~ic potentials over the current density range (Fig. 1C, F, I and L), implying ~~the always controlling of~~that the cathode rather than anode ~~for~~was controlling the performance of these ~~this~~ two-chamber MFC~~s~~ ~~performance as a function of~~over time. These results give clear evidence that the association of the deposited copper with the cathode surfaces alters the propensity of these materials for electricity generation and voltage output ~~over time~~~~during prolongued operation~~~~during prolongued operation~~ during prolonged operation.

3.2 Circuital current, Cu(II) removal and columbic efficiency (CE) over time

In general, both SSM and TS cathodes exhibited gradual increases in the circuital current (Fig. 2A), Cu(II) removal (Fig. 2B) and anodic CEs (Fig. 2C) over time. ~~There were~~The Cu(II) removal at cycle 12 was 99.7 ± 0.4% (SSM) and 87.7 ± 1.5% (TS) ~~of Cu(II) removal at cycle 12~~, which were as high as 1.28 (SSM) and 1.20 (TS) times of those in cycle 1. These results are in agreement with the results of the polarization tests (Fig. 1D, E, G and H). CR cathodes in cycle 1 had a low Cu(II) removal of 48.8 ± 1.9% (Fig. 2B) compared to the highest circuital current of 0.230 ± 0.001 mA (Fig. 2A), thus leading to low cathodic CEs (Fig. 2D). CS cathodes always showed the highest cathodic CEs than the others (Fig. 2D), ascribed to the lowest circuital current (Fig. 2A) and higher Cu(II) removal (Fig. 2B). Except CR, the observation of cathodic CEs with other material cathodes in excess of 100% at cycle 1 (Fig. 2D) indicates the occurrence of cathode corrosion, which was more significant in CS cathodes. The occurrence of cathode corrosion was mainly ascribed to the presence of Cl⁻ in the catholyte [25]. Other researchers also observed the corrosion of the cathodes or anodes in MFCs [26–28]. The decreasing cathodic CEs (Fig. 2D) and increasing Cu(II) reduction (Fig. 2B) for TS and SSM over consecutive cycles reflects the rates of corrosion decline and ~~of~~an increase in direct electron transfer. Thus, for TS and SSM, there was a shift away from corrosion to a predominantly cathodic Cu(II) reduction over time, although it was not possible to discern the relative contribution that these two different processes may have had on Cu(II) reduction. ~~No~~ Cu(II) was ~~measured~~not detected in the anolyte during these tests, although its existence in the cation exchange membrane ~~cannot~~could not be excluded [11].
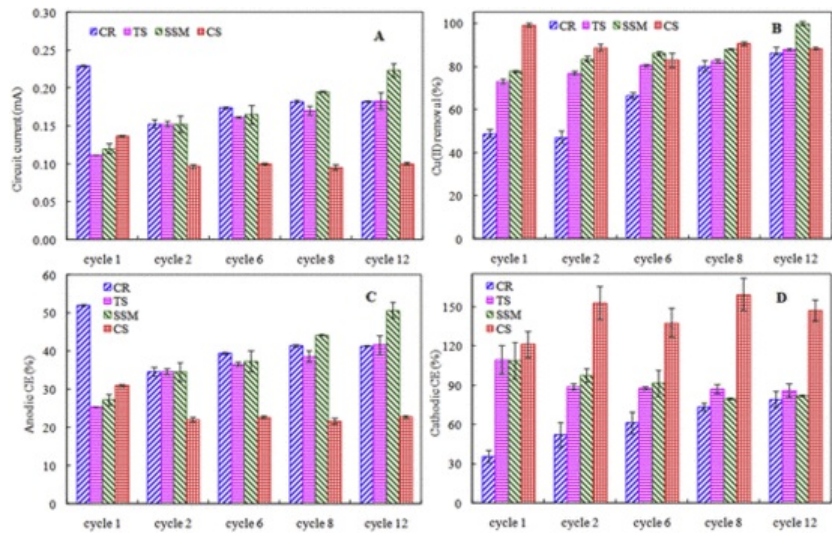
Fig. 2 Circuital current (A), Cu(II) removal (B), anodic CEs (C) and cathodic CEs (D) in MFCs with various material cathodes as a function of time.

The main advantage of using SSM cathodes in comparison to TS is the lower cost. The purchasing cost of the SSM used here was around 73 $ m^{-2}, compared to 450 $ m^{-2} for TS. In view of flexibility, SSM is certainly more suitable than CR for different MFCs configurations, producing a higher circuital current and a more efficient rate of Cu(II) reduction. Considering all the factors, this study shows that the SSM cathode has more advantages over the other cathode materials for application in larger-scale MFCs systems, showing the most appreciable rate of Cu(II) reduction, more flexibility than CR for different MFCs configurations, lower cost than TS, and much less corrosion than CS.

3.3 Electrochemical characterization using EIS

EIS spectra were fitted to equivalent circuits (Fig. S1) to identify the components of the internal resistances of the various cathode material cathodes atduring cycles 1 and 12 (Fig. 3). In cycle 1, TS hadexhibited a higher electrode resistance (629 Ω cm^2) than SSM (579 Ω cm^2), both of which were much higher than CR (169 Ω cm^2) and CS (143 Ω cm^2) (Fig. 4). In cycle 12, however, these values substantially decreased to 240 Ω cm^2 (TS) and 223 Ω cm^2 (SSM), both of which were similar to 223 Ω cm^2 for CR at the same cycle, explainingwhich explains the improved system performances of the TS and SSM cathodes over time (Figs. 1 and 2). In contrast, CR had a slight increase in resistance from an initial 169 Ω cm^2 to 223 Ω cm^2 at cycle 12, consistent with the low values in both circuital current (Fig. 2A) and Cu(II) removal (Fig. 2B). These results are supported by the observation of Zhang et al. [15], where a copper content of 12% increased the resistance of the substratum of activated carbon. Resistances of CS cathodes were always similarly low, mainly ascribed to the copper intrinsic characteristics of excellent conductor [10].
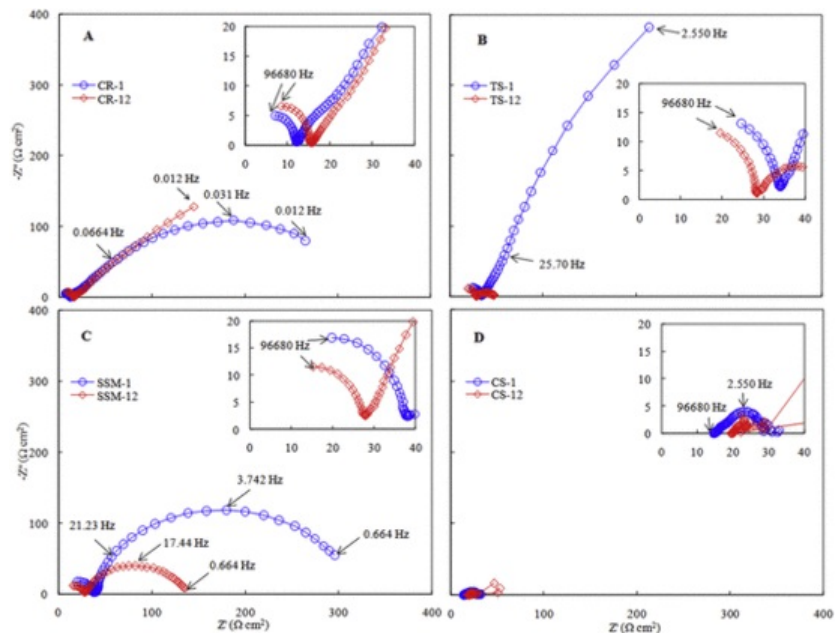
Fig. 3 Nyquist plots of EIS spectra by CR (A), TS (B), SSM (C), and CS (D) cathodes at cycles 1 and 12. Symbols represent experimental data, and lines represent data fit with the equivalent circuit.
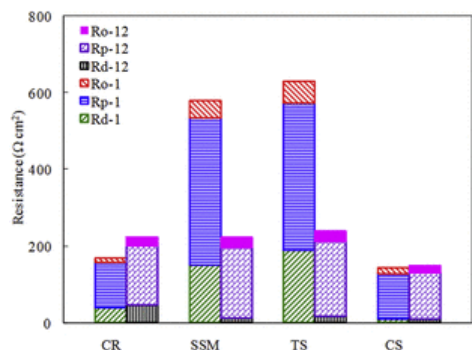

Fig. 4 Component analysis of internal resistance for different material cathodes at cycles 1 and 12.

The appreciable decrease in ~~D~~the diffusion resistance (R_d) ~~was was found to appreciably decrease within~~observed with the SSM and TS cathodes at cycle 12 (Fig. 4), considerably contributed to the apparent decrease in internal resistance, consistent with previous reports of enhanced surface conductivity by deposited copper in conventional electrochemical processes [14–16]. Similarly, the polarization resistance (R_p) and ohmic resistance (R_o) with both SSM and TS cathodes also diminished with copper deposition over time. These results illustrate the favorable effect of the deposited copper ~~for less~~on lessening the internal resistance of the SSM and TS electrodes.

3.4 Electrochemical analysis of cathodes using LSV

A strong reduction peak at a potential of 0.08 V and a current of –5.95 mA was observed for TS cathode, followed by 0.08 V and –3.49 mA for SSM at the same cycle 12 (Fig. 5). These results support the finding of the circuital current (Fig. 2A) and Cu(ll) removal (Fig. 2B), where TS reached the highest, followed by SSM, and CR ~~had~~with the lowest. Much lower reduction peaks ~~on~~observed with the CR than TS and SSM at the same cycle 12 implies ~~less incorporative~~ a smaller interactional effect~~s~~ of the copper deposited ~~copper and~~on CR on the exchange current. Control experiments in the absence of deposited copper reported reduction peaks with much low~~er~~ currents, reflecting the tremendous importance of the deposited copper in ~~these~~developing high current peaks, consistent with the excellent conducting properties of copper.
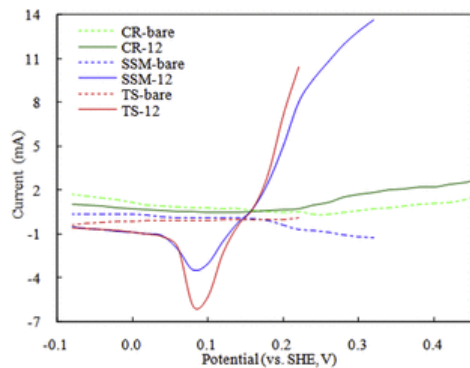
Fig. 5 LSV tests carried out on the various cathodes.

3.5 Morphology of the cathode and product confirmation

Compared to the bare cathodes of CR (Fig. 6A), TS (Fig. 6D), SSM (Fig. 6G) and CS (Fig. 6J), a layer of typical reddish-brown color of pure copper was observed on the electrodes ~~at the end~~after the completion of cycle 1 (Fig. 6B, E, H and K), implying the successful reduction of Cu(II) to pure copper on the surface of the various electrodes [3,5,9,19,20]. In contrast, the cathodes exhibited a darker appearance after exposure to air for 48 h (Fig. 6C, F, I and L), which resulted from the oxidation of metallic copper and the consequent alteration of both physical and electrochemical properties of the electrodes.

Fig. 6 Naked eye observation on CR (A, B and C), TS (D, E and F), SSM (G, H and I), and CS (J, K and L) cathodes. Fresh bare cathode (A, D, G and J) after the first cycle (B, E, H and K) and the subsequent exposure to air for 48 h (C, F, I and L).

The concentration of copper ion in solution with CS cathodes was further evaluated under ~~the~~ open circuit conditions and in the absence of Cu(II) in the catholyte. The concentration of Cu(II) in the catholyte at the end of the experiment was found to be 82 ± 1 mg L^{-1} with simultaneous reduction in the CS net weight by 22 ± 1 mg, confirming the occurrence of CS corrosion as the experiment proceeded. In parallel the color of the catholyte solution changed from colorless to light blue (Fig. S2). These results are in agreement by previous studies with MFCs using copper anodes or cathodes [10,27]. In contrast, no ~~any~~ color change was observed in the fresh catholyte under closed circuit conditions, illustrating the protecting role of cathodic electrons ~~in protecting~~on the surface of the sacrificial copper cathode in ~~the present~~this system.

Diverse nano-metric scale agglomerates were found on all cathodes of CR (Fig. 7A), TS (Fig. 7D), SSM (Fig. 7G) and CS (Fig. 7J) at the end of cycle 1, which provided a higher interfacial surface area for Cu(II) adsorption and an increase of the conductivity throughout the cathode [29]. Th~~is~~ese ~~results was~~wereobservations were in good agreement with the improved electricity generation (Fig. 1A, D and G) and circuital current (Fig. 2A) in the subsequent cycles. At the end of cycle 1, the distribution of copper nanoparticles on the surface of the CR cathode (Fig. 7A) ~~showed a~~was more uniform ~~distribution~~ than ~~those~~ on TS (Fig. 7D) and SSM (Fig. 7G) cathodes, mainly due to the high surface area of the carbon structure [18]. Rose-like (CR) (Fig. 7B), multi crystal (TS) (Fig. 7E) and cauliflower-like (SSM) (Fig. 7H) segregates were clearly observed after cycle 12, illustrating the importance of the cathode material on the diversity of shapes and morphology of the deposited copper [30–32]. The marked enhancement of the surface roughness after cycle 12 (Fig. 7B, E and H for CR, TS and SSM, respectively) in comparison to the smoother and compact surfaces after cycle 1 (Fig. 7A, D and G), led to an increase in the active surface area and, consequently, in the ~~measured~~observed power ~~production~~density (Fig. 1) and Cu(II) reduction (Fig. 2) [14]. In contrast, the CS cathode was severely corroded, resulting in remarkable sculptures on the surface, even after cycle 1 (Fig. 7J). More severe corrosion was reasonably observed on the CS cathode after cycle 12 (Fig. 7K). This result was similar to the corrosion of copper anodes, and Mn$_2$O$_3$ and copper cathodes in MFCs, as well as magnetite cathodes in MECs [26–28]. Although the size and shape of the copper particles deposited on these ~~various material~~ cathode~~s~~ materials were not tightly controlled, improvements in system performance were nonetheless observed, stressing the importance of the deposited copper on the cathode, particularly for subsequent cycles of Cu(II) reduction and electricity generation. A much deeper understanding of the issues affecting the morphology and nucleation of copper elements on the surfaces of each cathode materials is encouraged in further studies [31,32].
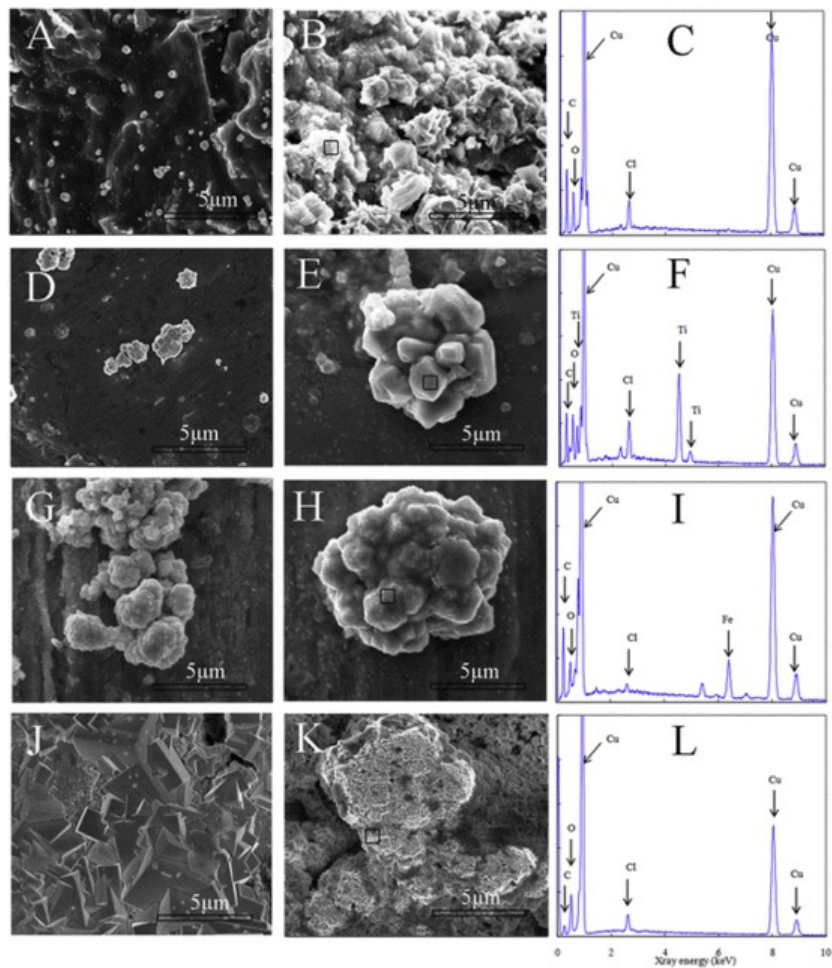
Fig. 7 SEM micrographs of the cathodes of CR (A and B), TS (D and E), SSM (G and H), and CS (J and K) at the end of cycle 1 (A, D, G and J) and cycle 12 (B, E, H and K). EDS analysis on products of Cu(II) reduction on the cathodes of CR (C), TS (F), SSM (I) and CS (L) at the end of cycle 1.

Further EDS analysis of the composition of the agglomerates, reported Cu signals at the same binding energies of 0.98, 8.06 and 8.87 keVs on the ~~cathodes of~~ CR (Fig. 7C), TS (Fig. 7F), SSM (Fig. 7I) and CS (Fig. 7L) cathodes, confirming the formation of Cu product. The observation of Cl signals on all the cathodes was associated with the catholyte of $CuCl_2$. Stronger Cl signals appeared on the CS after a prolonged operational time ~~of~~at cycle 12 (Fig. S3), confirming again the occurrence of a more severe corrosion of the surface. While copper was deposited on the ~~cathodes of~~ CR, TS and SSM cathodes, it may be necessary to use a settling clarifier ~~(setting)~~ to remove and peel off the copper precipitates from the electrodes ~~in order to~~if we were to achieve continuous copper removal in a practical system. Further investigations in this direction are certainly warranted.

The XRD patterns recorded on the CR, TS and SSM cathodes similarly and closely matched that of metal Cu^0 with standard peaks at 111, 200 and 220 ~~° degree~~ in 2θ (Fig. 8A), demonstrating the invariable products and their independence on these cathode materials.
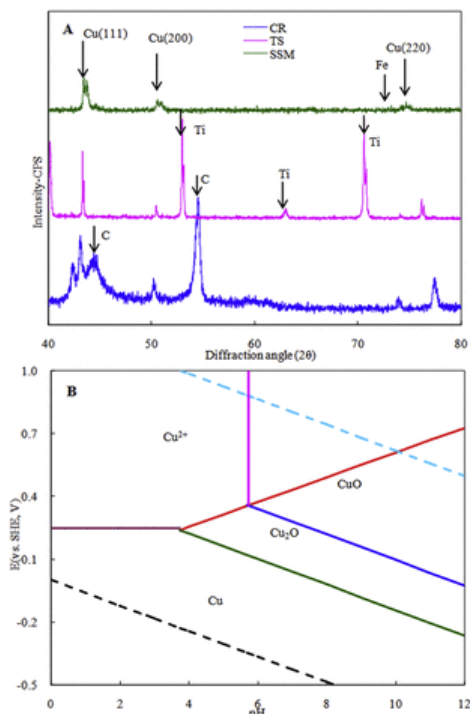
Fig. 8 (A) XRD determination on the cathodes of CR, TS and SSM after cycle 12. (B) Theoretical cathode potentials for half-reactions of Cu(II) to Cu(I), Cu(II) to Cu and Cu(I) to Cu at a Cu(II) of 50 mg L^{-1} and different pH values.

It is generally agreed that the copper products formed on the cathodes are pH dependent. Under the experimental temperature of 20 ± 3 °C and at an initial Cu(II) concentration of 50 mg L^{-1}, the theoretical cathode potentials of Cu(II) reduction at different pHs were calculated based on the Nernst equations (Fig. 8B). Considering the final pHs of 2.2–3.4 observed in the MFCs, ~~species of~~ the Cu(II) species in MFCs was reasonably reductively changed to pure copper under the present experimental conditions, further confirming the final products in this system (Fig. 8A).

Since Cu(II) laden wastewater generally comprise a range of multiple metal ions such as Cr(VI) and Cd(II) and others, future studies should focus on the impact of these other metals on the MFCs performance. The positive effects of the deposited copper on subsequent Cu(II) reduction and electricity generation, in the MFCs fitted with the CR, TS and SSM cathodes should be investigated in the presence of non-conductive metal deposits such as those from chromium and cadmium [22,33], to determine the most efficient cathode materials in industrial scale MFCs.

4 Conclusions

Copper recovery from aqueous Cu(II) is more attractive than treating and recovering other heavy metals due to its wide occurrence in acid mine drainage wastewaters. Previous studies have primarily examined the performance of carbon-based or copper plate cathode for Cu(II) reduction in MFCs. In this study we have examined a range of cathode materials on the effectiveness of Cu(II) reduction and electricity generation in MFCs in multiple operational cycles. The results shows the TS and SSM cathodes as the most effective for Cu(II) removal and power generation with the performance increasing over multiple cycles. This effect was associated to a reduction of the ohmic resistance over the cathodes and the increase in interfacial surface area of the cathode. This study gives a comprehensive appreciation of the effect of deposited copper on the various material cathodes, which further has a profound effect on the efficiency of Cu(II) reduction and electricity generation over time. Overall, the SSM was found the most promising cathode material considering the observed high performance and low material cost for use in practical MFCs. However, further studied should shed more light on the effect of concomitant heavy metal and their deposits on the overall performance of MFCs for water remediation and simultaneous production of renewable energy.

Acknowledgments

Appendix A. Supplementary data

Supplementary data related to this article can be found at http://dx.doi.org/10.1016/j.jpowsour.2016.01.022.

References

[1]

H. Wang and Z.J. Ren, *Water Res.* **66**, 2014, 219–232.

[2]

M. Bilal, J.A. Shah, T. Ashfaq, S.M.H. Gardazi, A.A. Tahir, A. Pervez, H. Haroon and Q. Mahmood, *J. Hazard. Mater.* **263**, 2013, 322–333.

[3]

S. Cheng, B. Wang and Y. Wang, *Bioresour. Technol.* **147**, 2013, 332–337.

[4]

A. ter Heijne, F. Liu, R. van der Weijden, J. Weijma, C.J.N. Buisman and H.V.M. Hamelers, *Environ. Sci. Technol.* **44**, 2010, 4376–4381.

[5]

H. Tao, M. Liang, W. Li, L. Zhang, J. Ni and W. Wu, *J. Hazard. Mater.* **189**, 2011, 186–192.

[6]

H. Tao, W. Li, M. Liang, N. Xu, J. Ni and W. Wu, *Bioresour. Technol.* **102**, 2011, 4774–4778.

[7]

H. Tao, L. Zhang, Z. Gao and W. Wu, *Bioresour. Technol.* **102**, 2011, 10334–10339.

[8]

Q. Zhang, Z. Wei, C. Liu, X. Liu, X. Qi, S. Chen, W. Ding, Y. Ma, F. Shi and Y. Zhou, *Inter. J. Hydrogen Energy* **37**, 2012, 822–830.

[9]

Z. An, H. Zhang, Q. Wen, Z. Chen and M. Du, *Desalination* **346**, 2014, 115–121.

[10]

P.R. Motos, A. er Heijne, R. van der Weijden, M. Saakes, C.J.N. Buisman and T.H.J.A. Sleutels, *Front. Microbiol.* **6**, 2015, http://dx.doi.org/10.3389/fmicb.2015.00527.

[11]

Y. Zhang, L. Yu, D. Wu, L. Huang, P. Zhou, X. Quan and G. Chen, *J. Power Sources* **273**, 2015, 1103–1113.

[12]

Q. Modin, X. Wang, X. Wu, S. Rauch and K.K. Fedje, *J. Hazard. Mater.* **235–236**, 2012, 291–297.

[13]

H. Luo, G. Liu, R. Zhang, Y. Bai, S. Fu and Y. Hou, *J. Hazard. Mater.* **270**, 2014, 153–159.

[14]

A.L. Rosa-Toro, R. Berenguer, C. Quijada, F. Montilla, E. Morallón and J.L. Vázquez, *J. Phys. Chem. B* **110**, 2006, 24021–24029.

[15]

L. Zhang, S.L. Candelaria, J. Tian, Y. Li, Y. Huang and G. Cao, *J. Power Sources* **236**, 2013, 215–223.

[16]

S. Zhang, H. Ma, L. Yan, W. Cao, T. Yan, Q. Wei and B. Du, *Biosens. Bioelectron.* **59**, 2014, 335–341.

[17]

Z.Y. Tian, H.J. Herrenbrück, P.M. Kouotou, H. Vieker, A. Beyer, A. Gölzhäuser and K. Kohse-Höinghaus, *Surf. Coat. Technol.* **230**, 2013, 33–38.

[18]

M. Ghasemi, W.R.W. Daud, M. Rahimnejad, M. Rezayi, A. Fatemi, Y. Jafari, M.R. Somalu and A. Manzour, *Inter. J. Hydrogen Energy* **38**, 2013, 9533–9540.

[19]

D. Wu, Y. Pan, L. Huang, X. Quan and J. Yang, *Chem. Eng. J.* **266**, 2015, 121–132.

[20]

D. Wu, Y. Pan, L. Huang, P. Zhou, X. Quan and H. Chen, *Sep. Purif. Technol.* **147**, 2015, 114–124.

[21]

S. Cheng, D. Xing, D.F. Call and B.E. Logan, *Environ. Sci. Technol.* **43**, 2009, 3953–3958.

[22]

L. Huang, Q. Wang, L. Jiang, P. Zhou, X. Quan and B.E. Logan, *Environ. Sci. Technol.* **49**, 2015, 9914–9924.

[23]

S.J. Hong, S. Lee, J.S. Jang and J.S. Lee, *Energy Environ. Sci.* **4**, 2011, 1781–1787.

[24]

J. Winfield, I. Ieropoulos, J. Greenman and J. Dennis, *Bioelectrochemistry* **81**, 2011, 22–27.

[25]

G. Tansuğ, T. Tüken, E.S. Giray, G. Fındıkkıran, G. Sığırcık, O. Demirkol and M. Erbil, *Corros. Sci.* **84**, 2014, 21–29.

[26]

E. Martin, B. Tartakovsky and O. Savadogo, *Electrochim. Acta* **58**, 2011, 58–66.

[27]

X. Zhu and B.E. Logan, *J. Chem. Technol. Biotechnol.* **89**, 2014, 471–474.

[28]

M. Siegert, M.D. Yates, D.F. Call, X. Zhu, A. Spormann and B.E. Logan, *ACS Sustain. Chem. Eng.* **2**, 2014, 910–917.

[29]

J. Du, C. Catania and G.C. Bazan, *Chem. Mater.* **26**, 2014, 686–697.

[30]

J. Wei, P. Liang and X. Huang, *Bioresour. Technol.* **102**, 2011, 9335–9344.

[31]

X. Liu, W. Li and H. Yu, *Chem. Soc. Rev.* **43**, 2014, 7718–7745.

[32]

T.J. Knisley, L.C. Kalutarage and C.H. Winter, *Coord. Chem. Rev.* **257**, 2013, 3222–3231.
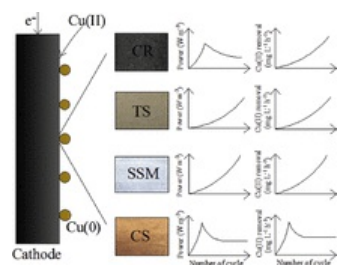
[33]

Q. Wang, Q.L. Huang, Y. Pan, P. Zhou, X. Quan, B.E. Logan and H. Chen, *Bioresour. Technol.* **200**, 2016, 565–571.

Appendix A. Supplementary data

The following is the supplementary data related to this article:

Multimedia Component 1

Graphical abstract

Highlights

- TS and SSM cathodes showed increased power production and Cu(II) removal over time.

- CR exhibited decreased power production and increased Cu(II) removal over time.

- TS and SSM cathodes exhibited a reduction of ohmic resistance over time.

Queries and Answers

Query: Please check the given name and surname of the author "Gianluca Li Puma", and correct if necessary.

Answer: Yes, the present expression is correct. The first name is "Gianluca" and the surname is "Li Puma"

Query: Please note that author's telephone/fax numbers are not published in Journal articles due to the fact that articles are available online and in print for many years, whereas telephone/fax numbers are changeable and therefore not reliable in the long term.

Answer: Okay, we understand this issue.

Query: Please confirm that given names and surnames have been identified correctly.

elsevier_POWER_22174

Answer: Yes, all of the given names and surnames have been correctly spelled.

Query: Your article is registered as a regular item and is being processed for inclusion in a regular issue of the journal. If this is NOT correct and your article belongs to a Special Issue/Collection please contact a.rassette@elsevier.com immediately prior to returning your corrections.

Answer: Yes, our article is a regular item.